Original Article

Estimation of the Proton Resonance Frequency Coefficient in Agar-based Phantoms

Antria Filippou, Nikolas Evripidou, Andreas Georgiou, Anastasia Nikolaou, Christakis Damianou

Department of Electrical Engineering, Computer Engineering and Informatics, Cyprus University of Technology, Limassol, Cyprus

Abstract

Aim: Agar-based phantoms are popular in high intensity focused ultrasound (HIFU) studies, with magnetic resonance imaging (MRI) preferred for guidance since it provides temperature monitoring by proton resonance frequency (PRF) shift magnetic resonance (MR) thermometry. MR thermometry monitoring depends on several factors, thus, herein, the PRF coefficient of agar phantoms was estimated. **Materials and Methods:** Seven phantoms were developed with varied agar (2, 4, or 6% w/v) or constant agar (6% w/v) and varied silica concentrations (2, 4, 6, or 8% w/v) to assess the effect of the concentration on the PRF coefficient. Each phantom was sonicated using varied acoustical power for a 30 s duration in both a laboratory setting and inside a 3T MRI scanner. PRF coefficients were estimated through linear trends between phase shift acquired using gradient sequences and thermocouple-based temperatures changes. **Results:** Linear regression ($R^2 = 0.9707–0.9991$) demonstrated a proportional dependency of phase shift with temperature change, resulting in PRF coefficients between −0.00336 ± 0.00029 and −0.00934 ± 0.00050 ppm/°C for the various phantom recipes. Weak negative linear correlations of the PRF coefficient were observed with increased agar. With silica concentrations, the negative linear correlation was strong. For all phantoms, calibrated PRF coefficients resulted in 1.01–3.01-fold higher temperature changes compared to the values calculated using a literature PRF coefficient. **Conclusions:** Phantoms developed with a 6% w/v agar concentration and doped with 0%–8% w/v silica best resemble tissue PRF coefficients and should be preferred in HIFU studies. The estimated PRF coefficients can result in enhanced MR thermometry monitoring and evaluation of HIFU protocols.

Keywords: Agar, magnetic resonance imaging, phantoms, silicon dioxide, thermometry, ultrasound

Received on: 26-10-2023 **Review completed on:** 26-01-2024 **Accepted on:** 27-03-2024 **Published on:** 25-06-2024

Introduction

Phantoms developed with tissue mimicking materials possess a pivotal role in the medical field in that they can be tailored to accurately mimic specific properties of human tissue, thus serving as tools in the evaluation of existing and emerging diagnostic and therapeutic medical systems.[1,2] Phantoms were initially introduced in the 1960s for calibrating diagnostic ultrasound (US) systems[3] and have thenceforth been abundantly developed with specific inclusion materials in homogeneous or anthropomorphic forms, in both research and commercial states, resembling specific biological tissues and tailored to certain medical applications.[2,3] In this regard, phantoms enable accurate and cost-effective quality assurance, quality control and efficacy validation of preclinical or clinical systems, minimizing the need for animal and human subjects.[2,4] Consequently, the ever-increasing development of novel therapeutic high-intensity focused ultrasound (HIFU) systems and applications[5] has been associated with an increased development of phantoms dedicated for use with HIFU validation studies.[2]

Phantoms tailored for HIFU feasibility studies should ideally emulate human tissue acoustic and thermal properties[6] as well as possess tissue-like properties encountered in magnetic resonance imaging (MRI).[7] Remarkably, the Onda Corporation (Sunnyvale, California, USA) company possesses a monopoly on the only commercially available phantom particularly suited for HIFU applications.[2] Although this phantom is manufactured with a polyacrylamide (PAA) gelling

Access this article online

Quick Response Code:

Website: www.jmp.org.in

DOI: 10.4103/jmp.jmp_146_23

Address for correspondence: Prof. Christakis Damianou, Department of Electrical Engineering, Computer Engineering and Informatics, Cyprus University of Technology, 30 Archbishop Kyprianou Street, Limassol 3036, Cyprus.
E-mail: christakis.damianou@cut.ac.cy

How to cite this article: Filippou A, Evripidou N, Georgiou A, Nikolaou A, Damianou C. Estimation of the proton resonance frequency coefficient in agar-based phantoms. J Med Phys 2024;49:167-80.

agent that provides transparency and locally turns opaque upon exposure to specific temperature thresholds, it possesses fixed acoustic and thermal properties.[2] Contrary, in-house developed water-based phantoms for HIFU applications can be fabricated with appropriate additives that individually adjust certain properties,[8-10] thus specifically emulating the tissue of interest. PAA is considered a favored gelling agent for developing phantoms for HIFU applications since it possesses a high melting temperature[11] and results in transparent phantoms[8,9,12,13] that permit visual assessment of the efficacy of the HIFU system under investigation. Nevertheless, PAA phantoms are toxic during the fabrication process,[8] with the developed phantoms exhibiting limited lifetime if not properly stored.[14] Gelatin is another gelling agent preferred in the custom development of phantoms, with additional inclusions employed to appropriately adjust specific phantom properties.[15-17] Nevertheless, although gelatin-based phantoms are manufactured in an easy and cost-effective manner,[16] their employment in HIFU exposures is only subjected to the application of low acoustic power,[16] accounting for the low melting temperature of gelatin.[4]

Contrary, agar is considered the most popular material for custom fabrication of phantoms dedicated to thermal therapies and HIFU applications since it is nontoxic and possesses a high melting point.[4] Silicon dioxide[18] and evaporated milk[19] are often used as additional ingredients to increase the acoustic attenuation[18] and absorption of the developed phantoms,[19] respectively. Increased concentrations of agar, silicon dioxide, and evaporated milk can independently enhance the acoustic properties of the agar-based phantoms to soft-tissue levels,[19] while simultaneously adjusting the magnetic properties[20] of these phantoms. Moreover, these materials can adjust the thermal properties of agar-based hydrogels, thus mimicking soft tissue,[6] while the addition of alcohols was recently reported in this sense for adjusting the thermal properties to fat tissue levels.[21] Given the popularity of agar, many studies have concentrated around the development of agar-based phantoms dedicated to HIFU feasibility studies,[22-24] with silicon dioxide and evaporated milk in appropriate concentrations reported for the development of anthropomorphic breast[23] and head[22] phantoms exhibiting tissue-like properties,[22,23] intended for the evaluation of breast-specific HIFU systems[23] and HIFU brain applications,[22] respectively.

HIFU systems and therapeutic protocols are normally guided by either US or MRI systems that provide visual monitoring of the procedure.[5] MRI is preferred as a guidance modality since it exhibits higher tissue image resolution than US[25] and enables the utilization of MRI thermometry tools for monitoring the temperature of the tissue.[26] Most MRI thermometry tools employed for monitoring MRI-guided focused ultrasound (MRgFUS) procedures are based on the temperature-dependent proton resonance frequency (PRF) shift technique,[26,27] that is in turn related to tissue temperature-induced changes observed in the hydrogen bonds.[26,27] Specifically, increased tissue temperatures arising during HIFU or other thermal exposures result in increased electron screening that in turn reduces the PRF and ultimately induces a phase shift in the detected MRI signal.[26,27] Therefore, PRF-based magnetic resonance (MR) thermometry provides quantitative temperature mapping by relating phase measurements of MR images acquired before and throughout thermal procedures, to tissue temperature changes.[26,27] Notably, these temperature and phase changes are further related to the magnetic field strength, the acquisition parameters of the MR imaging sequence and the PRF temperature change tissue coefficient.[26,27] The PRF tissue coefficient describes the linear temperature dependence of the PRF and is normally taken as a standard value of − 0.010 ppm/°C.[27] Nevertheless, calibration experiments are sometimes performed to accurately derive the PRF coefficient of the tissue under investigation and utilize the calibrated value in MR thermometry temperature monitoring. Similar methods are often employed for calibrating the PRF coefficient, wherein the investigated tissue is thermally heated, and the value is quantitatively acquired from the slopes of linear relationships arising between temperature and phase shift measurements.[28-38] Table 1 lists the PRF coefficients of various tissues and tissue substitutes as calibrated in published literature studies.[28-34,36-47]

The PRF coefficient is generally considered independent of tissue type following *ex vivo* animal tissue calibrations over a 20°C–80°C temperature range.[28] Excised rabbit and porcine kidney, brain, liver, and muscle tissues heated with a water bath over this temperature range within a 1.5 T MRI scanner, with temperature measurements simultaneously acquired using fiber-optic probes, resulted in approximately similar PRF coefficients for the various tissue types.[28] Contrary, analogous measurements performed inside a 7 T MRI scanner during *in vivo* microwave heating of rabbit muscle tissues resulted in a lower calibrated PRF coefficient[29] that was similar to the corresponding PRF coefficient of *in vivo* porcine muscle tissue as measured at 0.5 T during radiofrequency heating.[30] Notably, *in vivo* focused US heating of rabbit muscle tissue over a temperature range of 37°C–60°C inside a 1.5 T scanner reported an even lower PRF coefficient,[31] while similar temperature sensitivities were reported for *in vivo* rabbit brain tissues at 1.5 T following laser[32] and microwave heating[33] over the corresponding temperature ranges. Accordingly, *in vivo* radiofrequency heating of canine brain and muscle tissues over hyperthermic temperatures resulted in similar temperature sensitivities between the two tissue types.[34] Further inconsistencies in the calibrated PRF coefficients were reported for other *in vivo* studies in canine brain[35] and rabbit muscle[36] and brain[37,38] tissues possibly attributed to physiological tissue differences and discrepancies in the experimental calibration procedure,[28] while some deviations from linearity between the PRF shift and the temperature change have also been reported.[39] The results for the PRF coefficients of the aforementioned studies are summarized in Table 1.

Contrary to tissues, agar-based phantoms offer excellent linear thermal response of the PRF shift, thus making them

Table 1: Literature data of proton resonance frequency coefficients of various animal tissues and tissue mimicking phantoms

Tissue under investigation	Type	Calibrated PRF coefficient (ppm/°C)	Reference
Animal tissues			
Rabbit and porcine kidney, brain, liver, and muscle	*Ex-vivo*	−0.010–−0.0105 (average: −0.0101±0.0004)	[28]
Porcine liver	*Ex-vivo*	−0.0073–−0.0080	[39]
Rabbit muscle	*In-vivo*	−0.00976	[29]
Porcine muscle	*In-vivo*	−0.009±0.001	[30]
Rabbit muscle	*In-vivo*	−0.007±0.001	[31]
Rabbit brain	*In-vivo*	−0.0088±0.0001	[32]
Rabbit brain	*In-vivo*	−0.008	[33]
Canine brain	*In-vivo*	−0.00695	[34]
Canine muscle	*In-vivo*	−0.00674	[34]
Rabbit muscle	*In-vivo*	−0.00909	[36]
Rabbit brain	*In-vivo*	−0.0098±0.0005	[37]
Rabbit brain	*In-vivo*	−0.0107±0.0009	[38]
Phantoms			
Agar phantom	Composition: 2% agar	−0.01–−0.0105	[28]
Agar phantom	Composition: 2% agar, 0.25 mm Gd-DTPA, 0.9% NaCl, 0.05% NaN_3	−0.00977	[29]
Agar phantom	Composition: 1.5% agar	−0.011±0.001	[30]
Agar phantom	Composition: 2% agar, nickel nitrate	−0.0085±0.0002	[39]
Agar phantom	Composition: 2% agar	Parallel orientation: −0.0094±0.0001 Perpendicular orientation: −0.0055–−0.0130 (average: −0.0098±0.0004)	[40]
Agar phantom	Composition: 2% agar, 0.05% black ink	5 mm slice thickness: −0.0104±0.0001 10 mm slice thickness: −0.0084±0.0001	[41]
Agar phantom	Composition: 1% agar	−0.0095	[42]
PAA phantom	Composition: -	MRI scanner: −0.0083 Spectroscopic: −0.0091±0.0007	[43]
PAA phantom	Composition: 37.9% water, 30% rotiphorese, 16% BSA, 10% PVA microsphere, 0.04% Magnevist, 3.3% lumirem, 0.08% TEMED, 1.75% APS, 0.9% NaCl, 0.03% NaN_3	−0.0088±0.0002	[44]
PAA phantom	Composition: 19.11 g citric acid, 29.57 g sodium citrate tribasic dihydrate, 30.8% BSA, 70 g acrylamide, 1.4 g bis-acrylamide, 30% intralipid	−0.0095±0.0005	[45]
Gelatin phantom	Composition: 90% aqueous gelatin, 10% vegetable oil, 6 g saline	−0.0104±0.0003	[46]
Gelatin phantom	Composition: 73.5% water, 13.72% gelatin, 8.52% sunflower oil, 0.46% surfactant, 0.6% NaCl, 3.19% formaldehyde	−0.0123	[47]

PRF: Proton resonance frequency, PAA: Polyacrylamide, MRI: Magnetic resonance imaging, BSA: Bovine serum albumin, PVA: Polyvinyl acetate, APS: Ammonium persulfate, TEMED: Tetramethylethylenediamine, Gd-DTPA: Gadolinium-diethylenetriamine penta-acetic acid

suitable tools for employment with the PRF method[39] which is considered the most accurate temperature monitoring modality in agar-based phantoms.[48] Nevertheless, PRF coefficient dependencies have been described with magnetic susceptibility changes attributed to the orientation and spatial distribution of thermal heating relative to the magnetic field.[40] Experimental studies performed for water bath heated agar-based phantoms within a 1.5 T clinical MRI scanner revealed PRF coefficient variations for thermal heating distribution in planes parallel and perpendicular to the magnetic field orientation, resulting in up to 30% deviations in MR thermometry-based temperature measurements in case such dependencies are disregarded.[40] Accordingly, PRF calibrations of agar-based phantoms doped with black ink during laser heating, with the heating source aligned parallel to the main magnetic field and temperatures concurrently acquired with fiber-optic probes, resulted in a decrease in the PRF coefficients for a 2-fold increase in the slice thickness of the imaging sequence, attributable to volume averaging effects in the phase measurements arising with the increased slice thickness.[41] The PRF coefficients for these studies are also included in Table 1.

Over the years, researchers have experimentally calibrated the PRF coefficient of phantoms developed with various gelling agents to improve the accuracy of PRF MR thermometry monitoring.[28-30,39-47] Olsrud *et al.*[39] developed 2% agar-based phantoms doped with nickel nitrate that were heated to

temperatures in the 25°C–80°C range by means of a water bath, while being scanned within a 1.5 T MRI scanner and derived the PRF coefficient from simultaneous phase difference and thermocouple-based temperature change measurements. Similar utilization of a water bath[28] and microwave applicators[29] for heating agar-based phantoms having the corresponding agar concentration (2%) were also performed inside 1.5 T[28] and 7 T[29] scanners. Recently, Wang[42] performed agar-phantom-based PRF coefficient calibrations for executing MR thermometry calculations at 7 T, wherein MRI-compatible thermocouples were inserted within a hollow annular agar-based phantom, while hot water was introduced within the hollow area to increase the temperature of the phantom. The PRF coefficient of the phantom was calculated from a typical linear relationship fitted between phase shifts and temperature changes arising from MR images and concurrent thermocouple measurements acquired during heating, respectively.[42] Accordingly, PRF coefficient measurements were reported for muscle-like PAA phantoms from a linear trend existing between sensor-based temperature change measurements in the range of 20°C–55°C and phase shifts of images acquired at 1.5 T during microwave heating using either a clinical MRI scanner or spectroscopic techniques.[43] In another study,[44] employment of a 1.5 T scanner for imaging and fiber-optic probes for temperature measurements during laser heating were reported for calibrating the PRF coefficient of another acrylamide phantom doped with bovine serum albumin (BSA). Lochhead *et al*.[45] utilized a previously developed PAA-based phantom doped with BSA protein[10] to calibrate it for MRgFUS studies and examine its PRF temperature dependencies by simultaneously acquiring sensor-based temperature measurements and MR images at 1.5 T during focused US heating.[45] Appropriately, PRF coefficients were also reported for oil-in-gelatin phantoms from phase shifts at 1.5 T and temperature measurements acquired with single[46] and multiple[47] temperature sensors, being similar to the PRF coefficient of a 1.5% agar-based phantom as calculated for radiofrequency heating at 0.5 T.[30] Details regarding the PRF coefficients of these phantoms are found in Table 1.

Considering that accurate PRF MR thermometry temperature calculations are dependent on the PRF coefficient,[40,47] PRF coefficient calibrations of several agar-based phantoms were executed in the present study, following their vast development and use in HIFU validation studies.[18-24] This study is inspired by an observed gap in existing literature relating to the effect of the inclusions of agar-based phantoms on the PRF coefficient. Following previous studies that reported the effect of different concentrations of agar and silicon dioxide on the acoustic[6,19] and magnetic[20] properties of fabricated agar-based phantoms, the phantoms herein were developed with varied concentrations of agar or silicon dioxide to assess the effect of the varying concentrations on the calibrated PRF coefficient. A series of identical HIFU exposures was executed on the agar-based phantoms within a 3 T clinical MRI environment and in a laboratory setting. Given the excellent linear thermal response agar-based phantoms exhibit with the PRF technique,[39] the PRF coefficient of each phantom was estimated through the linear relationships taken between temperature and phase shift measurements acquired from the laboratory and MRI HIFU exposures, respectively. Subsequently, MR thermometry calculations were performed for the HIFU exposures to assess the effect of the calibrated PRF coefficients on the temperature measurements.

Materials and Methods

Agar-based phantoms

Initially, three agar-based phantoms were developed with varied percentage weight per volume (w/v) concentrations of agar (101614, Merck KGgA, Darmstadt, Germany) to examine any dependency of the PRF temperature coefficient with the agar concentration. In this regard, the agar-based phantoms were individually developed with 2, 4, or 6% w/v agar concentrations following the fabrication procedure previously mentioned by Drakos *et al*.[19] Briefly, 510 ml of pure, deionized and degassed water were steadily heated by means of a glass beaker that was accommodated on a magnetic hotplate (SBS A160, Steinberg Systems, Hamburg, Germany). A magnetic stir bar immersed in the water volume, interacted with the magnetic hotplate (SBS A160, Steinberg Systems) and provided continuous stirring of the water throughout heating. The appropriate % w/v agar concentration (2, 4 or 6) was grinded into a fine powder that was added in the water when its temperature, as recorded with a digital thermometer (HH806AU, Omega Engineering, Connecticut, USA) reached 50°C. Thereafter, the agar water solution was continuously heated while concurrently being magnetically stirred until the temperature of the solution exceeded 85°C, whereupon the heating function of the magnetic hotplate (SBS A160, Steinberg Systems) was switched off and the solution was allowed to cool to approximately 50°C while undergoing continuous magnetic stirring. Subsequently, the solution was poured into 3D-printed (FD270, Stratasys, Minnesota, USA) cuboid molds with dimensions of 80 mm (w) ×90 mm (l) ×70 mm (h) and was allowed to solidify within a refrigerator.

Thereafter, four agar-based phantoms doped with silicon dioxide (Sigma-Aldrich, Missouri, USA) were developed with a constant 6% w/v concentration of agar and varied % w/v silicon dioxide concentration (2, 4, 6, or 8% w/v) to investigate any effect of the increased silicon dioxide concentration on the PRF temperature coefficient. Notably, the four phantoms were fabricated following the above-mentioned preparation process utilizing identical water volumes and heating temperature thresholds, with the development process only differing in the addition of silicon dioxide in the agar-water solution. Silicon dioxide was appropriately added with the correct concentration (2, 4, 6, or 8% w/v) in the solution, within a short timeframe following the addition of agar (6% w/v). The agar-based silicon dioxide doped solutions were individually poured in the aforementioned 3D-printed molds (FD270,

Stratasys) and were placed in the refrigerator to undergo jellification. Notably, before experimental studies, the seven phantoms were removed from the molds and were allowed to reach ambient temperature.

Features of robotic system for MRI-guided focused ultrasound ablations

An MRgFUS robotic system was selected from a range of existing robotic systems developed for preclinical MRgFUS applications.[49-55] Remarkably, the existing robotic systems have all been fabricated with MRI-compatible materials enabling proper operation within clinical MRI scanners and uninfluenced MR imaging for monitoring sonications.[49-55] Specifically, the selected MRgFUS robotic system[49] was fabricated with Acrylonitrile Styrene Acrylate (ASA) thermoplastic using a 3D-printer (FD270, Stratasys) and provides mechanical computer-controlled linear motion in three axes (X, Y, and Z). Notably, MRI-compatible piezoelectric motors (USR60-S3N, Shinsei Kogyo Corporation, Tokyo Japan) coupled to linear optical encoders (US Digital, Vancouver, Washington, USA) are employed to initiate and precisely control linear motion, respectively.[49] Motion is transferred to a single-element concave transducer with a diameter of 50 mm operating at a frequency of 2.75 MHz and focusing at 65 mm, that frontally extends from the positioning mechanisms to a water-filled container. It is worthmentioning that the water-filled container is fitted with an opening, thus allowing the ultrasonic beam to be transmitted from the transducer to the targeted subject, through the deionized and degassed water medium.

Control software for high-intensity focused ultrasound exposures

The MRgFUS robotic system interfaces with an in-house software developed in C# (Visual Studio, Microsoft Corporation, Washington, USA) that controls the parameters of the HIFU exposures.[56] Specifically, the operating frequency of the transducer, the amount of power delivered, and the sonication time can be arranged through suitable commands. In addition, the developed software allows interfacing with clinical MRI scanners for MR image transfer, thus enabling treatment monitoring through MR thermometry tools based on the PRF method.[26,27]

High-intensity focused ultrasound exposures within a magnetic resonance imaging environment

The MRgFUS robotic system was accommodated on the table of a 3 T clinical MRI scanner (Magnetom Vida, Siemens Healthineers, Erlangen, Germany), as shown in Figure 1. The phantoms were individually accommodated on the acoustic opening of the robotic system through a rigid 3D-printed (FD270, Stratasys) ASA phantom holder. The 3D-printed ASA phantom holder provided support for each phantom at the center of the acoustic opening so that ultrasonic beam directly propagated from the transducer to the center of the agar-based phantom. Similarly, a rigid ASA structure was accommodated on the MRI table, surrounding the robotic system, providing support to a multi-channel body

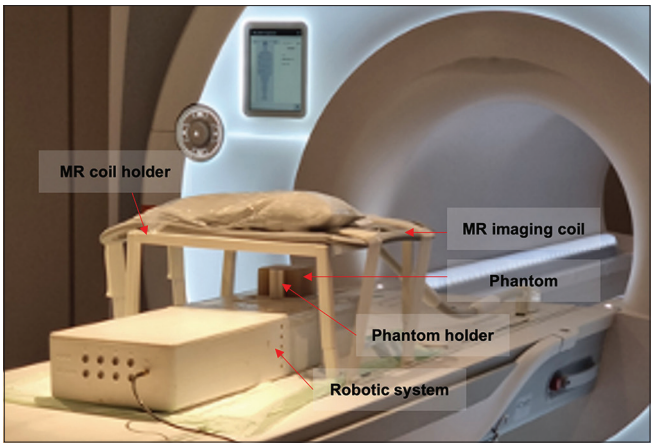

Figure 1: Experimental set-up with the robotic system accommodated on the table of a clinical magnetic resonance imaging scanner and an agar-based phantom positioned on the acoustic opening of the robotic system and a magnetic resonance imaging coil employed for image acquisition

MR imaging coil (Body18, Siemens Healthineers) on top of the agar-based phantom. The transducer was connected to an amplifier (AG1016, T and C Power Conversion, Rochester, NY, USA) and to the in-house developed software that was in turn interfaced with the MRI scanner for MR image acquisition.

Identical single-point sonications were individually executed on each of the seven agar-based phantoms. Each phantom was sonicated by applying varied acoustic power of 18, 24, 30, 36, and 42 W for a constant sonication time of 30 s at a focal depth of 25 mm. During the five individual sonications, MRI scans of each of the seven agar-based phantoms were performed in the coronal plane using the MR imaging body coil (Body18, Siemens Healthineers) and a Fast low angle shot (FLASH) sequence with the following acquisition parameters: Repetition time (TR) =25 ms, Echo time (TE) =10 ms, field of view = 280 mm × 280 mm, Slice thickness = 5 mm, Acquisition matrix = 96 × 96, Number of excitations = 1, Echo train length = 1, Flip angle = 30°, and Pixel bandwidth = 240 Hz/pixel. Notably, for each of the seven phantoms, three FLASH scans were performed before each individual HIFU exposure at varied acoustical power for acquisition of three reference images. Acquisition of images before each HIFU exposure was necessary for imaging the phantoms at baseline temperatures, while the number of reference images acquired (3) was essential to adjust for any irregularities of the FLASH pulse sequence. Correspondingly, FLASH images throughout the HIFU exposures were acquired at timeframes of 2.4 s for a total imaging time of 60 s, corresponding to 30 s sonication time and 30 s cooling time after the elapsed sonication time.

High-intensity focused ultrasound exposures in the laboratory environment

Following the HIFU exposures within the MRI environment, equivalent benchtop ultrasonic protocols were performed with the MRgFUS robotic system on the seven phantoms inside the laboratory setting. In this regard, each of the phantoms was individually accommodated in the acoustic opening of the

robotic system, through the 3D-printed (FD270, Stratasys) ASA phantom holder, in an equivalent manner to the experimental setting configuration within the MRI environment. It is worthnoting that the ASA phantom supporting structure, apart from providing rigid support to the phantom at the center of the acoustic opening, additionally permitted accurate insertion of thermocouples at every 5 mm within the phantom, in a plane perpendicular to the propagation of the ultrasonic beam, through small circular apertures vertically existing on the 3D-printed (FD270, Stratasys) structure.

The five sonication protocols defined by the varied acoustic power (18, 24, 30, 36, and 42 W) for the sonication time of 30 s at a focal depth of 25 mm were equivalently executed on the seven agar-based and agar-based doped with silicon dioxide phantoms. In this regard, a 100 μm thick thermocouple (5SRTC-TT-K-30-36, type K insulated beaded wire, Omega Engineering) was individually inserted within each of the seven agar-based phantoms at a 25 mm depth. The tip of the thermocouple was carefully inserted at the center of the phantom to directly measure the temperature at the focal point. The temperature induced resulting each ultrasonic exposure was recorded by the thermocouple and the digital thermometer (HH806AU, Omega Engineering) with a temporal resolution of 1 s. Accommodation of the phantoms on the 3D-printed ASA structure ensured that benchtop sonications on each of the phantoms were executed at the exact location where exposures within the MRI environment were performed. In this regard, experimental measurements acquired within the two environments (laboratory, and MRI) could be comparable.

Proton resonance frequency temperature change coefficient calculations

The calculations were performed to measure the temperature change coefficient (α) of each phantom developed with either varied agar or silicon dioxide concentrations, using the PRF method.[26,27] With the PRF technique, temperature changes (ΔT) within the tissue arising during exposure to thermal heating induce a shift in the PRF that is consequently observed as a phase difference ($\Delta\varphi$) in MR images acquired before and throughout HIFU exposures. The PRF technique relates these temperature changes to the phase difference through the following equation:

$$\Delta T = \frac{\varphi(T) - \varphi(T_0)}{\alpha\gamma B_0 TE} \quad (1)$$

where $\varphi(T)$ and $\varphi(T_0)$ are the phase of images acquired before (baseline tissue temperature) and during HIFU exposure (ablation temperature), respectively, γ is the gyromagnetic ratio, B_0 is the local magnetic field strength, and TE is the echo time of the employed MR imaging sequence.

In this regard, for temperature change coefficient (α) calculations, Equation 1 was rearranged into the following format, where all the variables have their abovementioned meanings:

$$\alpha = \frac{\Delta\varphi}{\Delta T\gamma B_0 TE} \quad (2)$$

For each of the five individual HIFU sonications executed on each of the seven agar-based phantoms, the phase difference ($\Delta\varphi$) was calculated from the FLASH images acquired for the HIFU exposures performed within the MRI environment. In this sense, the coronal magnitude and phase FLASH images of each of the seven agar-based phantoms acquired before (reference images) and during (ablation images) the varied HIFU exposures were loaded into a Digital Imaging and Communication in Medicine (DICOM) software (MicroDicom, MicroDicom Ltd., Sofia, Bulgaria) for postprocessing. On the individual phase FLASH images of each phantom, circular regions of interest (ROIs) with a diameter of 3 mm were set. The ROIs were arranged on all the images (reference and ablation) at the corresponding location of the focal spot, as visualized on the magnitude images acquired throughout the HIFU exposures, while the diameter of the ROIs (3 mm) was chosen after considerations related to the width of the focal beam.

Consequently, for phase images, the average signal intensity (SI) within the ROI was measured with the MicroDicom (MicroDicom Ltd.) software for the three reference images acquired before heating, as well as for the image acquired at the maximum ablation temperature during exposures. The SI measurements of the reference and ablation phase images were then converted to radians within the range of 0–2 π, by utilizing the minimum and maximum image pixel values as defined by the acquired DICOM image (minimum and maximum image pixel values of 0 and 4095, respectively), thus resulting in the phase values for the reference and ablation phase images. It is worth stating that the phase difference was then calculated by taking the absolute difference between the phase values of the ablation image and the average value of the individual phases of the three reference images.

Accordingly, for each of the five sonications executed on each developed phantom, the corresponding phase difference value was related to the maximum temperature change as recorded with the thermocouple during benchtop sonications performed in the laboratory setting. Consequently, graphical plots of the temperature change against the phase difference values, as calculated for each of the sonications executed at varied applied acoustic power, were individually generated for the seven phantoms. Eventually, regression analysis was performed and the PRF coefficient of each fabricated phantom was calculated by fitting the inverse of the slope of the regression analysis (i.e., $\Delta\varphi/\Delta T$) in Equation 2. Concerning the three remaining variables of the equation, the gyromagnetic ratio of the water proton γ was taken as 42.58 MHz/T, the magnetic field strength was set at 3 T, while a TE of 10 ms was utilized arising from the acquisition parameters of the employed FLASH sequence. Uncertainties in the PRF coefficient of each phantom were calculated by utilizing the error in the slope of the regression analysis and following error propagation formulae based on

Equation 2. It is worthstating that no errors were considered for constant variables (i.e., gyromagnetic ratio of the water proton, magnetic field strength, and TE).

Magnetic Resonance Thermometry Temperature Measurements

Following the calculations for the PRF coefficients of the seven agar-based phantoms, MR thermometry temperature estimations were executed based on the PRF technique[26,27] using the aforementioned in-house control software. The coronal FLASH images of the various agar-based phantoms acquired in the course of sonications executed at varied acoustic power (18, 24, 30, 36, and 42 W) for a constant sonication time (30 s) within the 3 T MRI scanner (Magnetom Vida, Siemens Healthineers) were processed by the in-house software to derive the temperature increase induced as a result of each individual sonication executed on each of the seven phantoms. The FLASH images of each phantom were processed by the software, and temperatures induced resulting from each sonication at varied acoustic power were calculated in a particular ROI within each phantom using PRF-based MR thermometry and Equation 1. Notably, for consistency and accuracy purposes, the ROI at which temperatures were estimated was set in each phantom with an identical size (diameter of 3 mm) at the corresponding locations where phase measurements for the PRF coefficient calibrations were executed. Initially, for each phantom, temperatures within the specific ROIs resulting each sonication executed at varied acoustical power were calculated utilizing the corresponding calibrated PRF coefficient. Subsequently, MR thermometry temperature estimations were additionally executed for each phantom and sonication, utilizing a PRF coefficient of −0.0094 ppm/°C that is typically reported in the literature for MR thermometry estimations in in-house gel phantoms[40,57,58] and is employed as a default value for the PRF coefficient by the in-house developed software. MR thermometry data, specifically color-coded thermal maps and timeseries plots of the temperature at the specified ROI were generated for each sonication and phantom using the calibrated and default values of the PRF coefficients to assess the effect of the calibrated coefficient on temperature measurements. It is worthstating that the color-coded thermal maps generated for each phantom and sonication were overlapped on the corresponding magnitude scans of the phantom, thus presenting the extent of thermal heating throughout the phantom during sonications.

Results

Proton resonance frequency temperature change coefficient calculations

Phase shift measurements as derived from the phase images of each of the seven agar-based phantoms acquired during sonications at varied acoustic power within the MRI environment were correlated with the maximum thermocouple measured temperature changes. Figure 2a and b show the characteristic graphical plots of a linear response of the temperature change with the phase shift at various sonication protocols executed on an agar-based phantom (6% w/v agar) and on the corresponding agar-based phantom doped with silicon dioxide (6% w/v agar and 6% w/v silicon dioxide), with the error bars indicating the uncertainties in the temperature change and phase shift measurements. Following least-squares, no intercept linear regression analysis between the temperature changes and phase difference values resulting the five sonications individually performed on each phantom, the PRF coefficient was estimated for the three agar-based phantoms and the four agar-based phantoms doped with silicon dioxide, as shown in Tables 2 and 3, respectively. Linear regression fits, statistical errors for the slope of the regression fits (δ_{slope}), and corresponding statistical errors for the calculated PRF coefficients for each phantom are also listed in Tables 2 and 3.

Figure 3a shows the effect of the varied agar concentration (2, 4, and 6% w/v) on the calibrated PRF coefficient of the three agar-based phantoms, where the error bars represent the uncertainties. Following linear regression analysis ($R^2 = 0.3741$), a weak inverse proportional effect on the PRF coefficient was observed with an increased concentration of agar. Accordingly, the effect of the varied concentration of silicon dioxide (2, 4, 6, or 8% w/v) on the calibrated PRF coefficient of the four agar-based phantoms (6% w/v) doped with silicon dioxide is shown in Figure 3b, with the

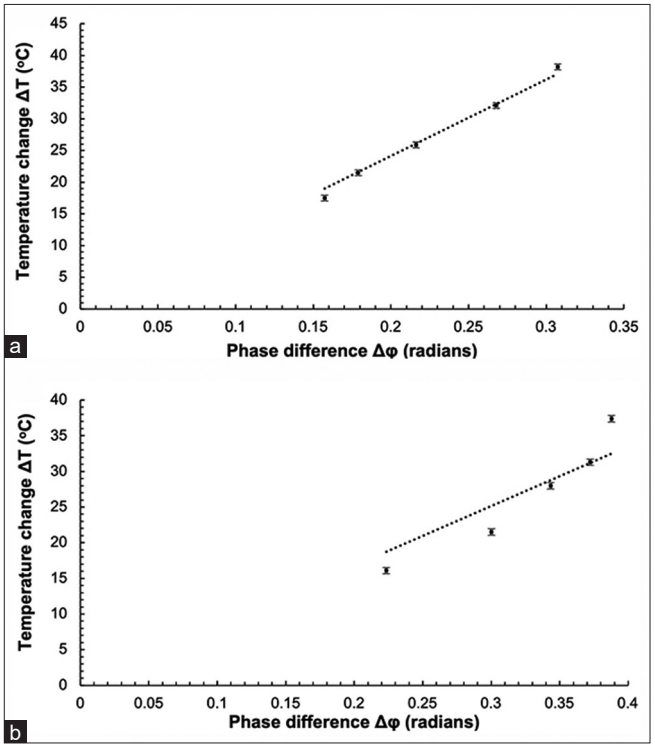

Figure 2: Plots of temperature change versus phase difference as calculated for sonications executed on (a) a 6% w/v agar-based phantom, and (b) a 6% w/v agar-based phantom doped with 6% w/v silicon dioxide using a 2.75 MHz transducer at varied acoustical power for a sonication time of 30 s at 25 mm focal depth

error bars indicating the statistical error. The calibrated PRF coefficient (−0.00649 ± 0.0001 ppm/°C) of the purely agar-based phantom developed with the corresponding agar concentration (6% w/v) without silicon dioxide (0% w/v) is also included in Figure 3b for comparison purposes. After least-squares linear regression fit with a Pearson correlation coefficient (R^2) of 0.7159, a strong negative correlation was observed between the PRF coefficient and increased concentration of silicon dioxide.

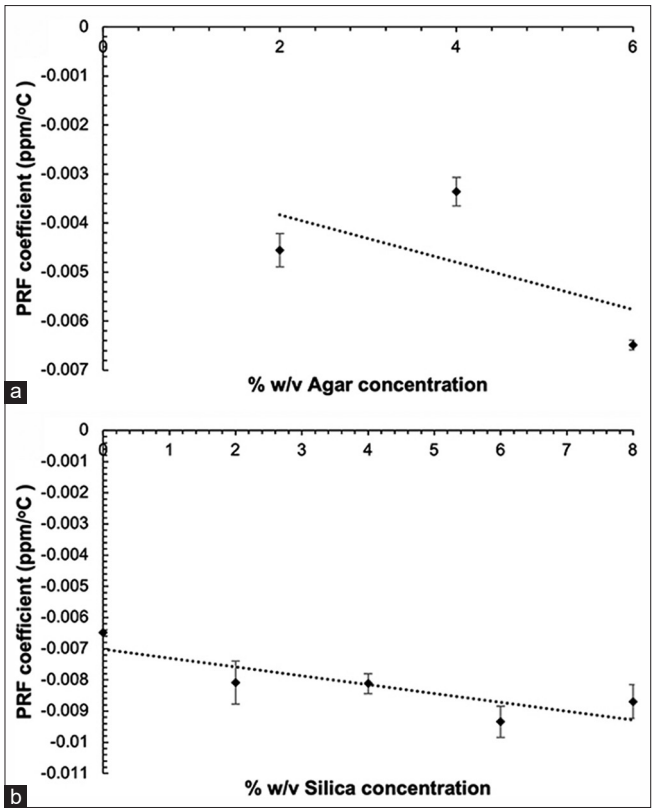

Figure 3: Proton resonance frequency temperature coefficients of (a) three agar-based phantoms developed with varied agar concentrations (2, 4, and 6% w/v), and (b) five agar-based phantoms (6% w/v agar) doped with varied silicon dioxide concentrations (0, 2, 4, 6, and 8% w/v)

Magnetic resonance thermometry temperature measurements

MR thermometry data produced for each phantom and sonication using either the respective calibrated or default PRF coefficients were generated every 2.4 s for the duration of the exposures, equivalent to the temporal resolution of the FLASH sequence. Figure 4a shows typical thermal maps generated in the coronal plane (perpendicular to the ultrasonic beam propagation) at the end of sonications (sonication time of 30 s) executed with a low acoustic power (24 W) on an agar-based phantom (6% w/v) using the corresponding calibrated PRF coefficient (−0.00649 ± 0.0001 ppm/°C) of the specific phantom. At the ROI specified within the agar-based phantom (6% w/v), a maximum temperature of about 59°C was recorded utilizing the calibrated PRF coefficient of the phantom, as shown in Figure 4b. Accordingly, Figure 5a shows the respective coronal thermal maps of the same agar-based phantom (6% w/v) generated at the identical timepoint for the equivalent ultrasonic protocols (acoustic power of 24 W for sonication time of 30 s at a 25 mm focal depth) by employing the default value of the PRF coefficient. Figure 5b shows a maximum temperature of approximately 52°C achieved at the corresponding ROI within the agar-based phantom (6% w/v) resulting sonications, as generated with MR thermometry based on the default value of the PRF coefficient. Tables 4 and 5 show the temperature changes, from a reference

Table 2: Proton resonance frequency temperature coefficient of agar-based phantoms having varied concentrations of agar as calibrated resulting sonications executed with a 2.75 MHz transducer at varied acoustical power for a sonication time of 30 s at 25 mm focal depth

Agar content (% w/v)	Linear regression	δ_{slope}	Pearson correlation coefficient (R^2)	PRF temperature coefficient±statistical error (ppm/°C)
2	y=171.82x	12.841	0.9781	−0.00456±0.00034
4	y=233.16x	20.237	0.9707	−0.00336±0.00029
6	y=120.65x	1.803	0.9991	−0.00649±0.0001

PRF: Proton resonance frequency

Table 3: Proton resonance frequency temperature coefficient of agar-based phantoms doped with varied concentrations of silicon dioxide as calibrated resulting sonications executed with a 2.75 MHz transducer at varied acoustical power for a sonication time of 30 s at 25 mm focal depth

Agar=6% w/v, silica content (% w/v)	Linear regression	δ_{slope}	Pearson correlation coefficient (R^2)	PRF temperature coefficient (ppm/°C)
2	y=96.765x	8.235	0.9718	−0.00809±0.00069
4	y=96.47x	3.780	0.9939	−0.00811±0.00032
6	y=83.783x	4.526	0.9885	−0.00934±0.00050
8	y=90.023x	5.550	0.985	−0.00869±0.00054

PRF: Proton resonance frequency

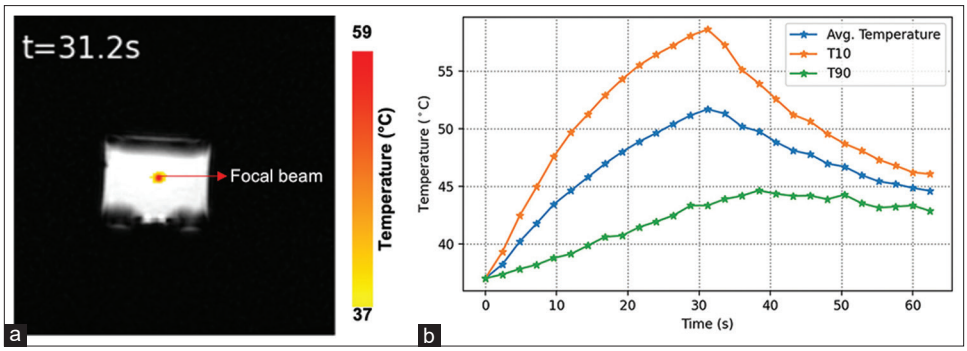

Figure 4: (a) Coronal thermal maps acquired at the end of sonications (acoustic power of 24 W for 30 s at 25 mm focal depth) executed on an agar-based phantom (6% w/v), and (b) Timeseries temperature increase at the focal spot during sonications, as calculated using the calibrated PRF coefficient of the phantom

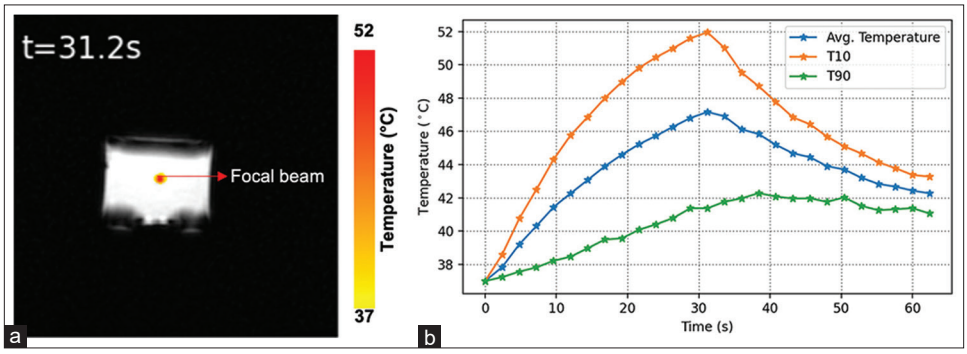

Figure 5: (a) Coronal thermal maps acquired at the end of sonications (acoustic power of 24 W for 30 s at 25 mm focal depth) executed on an agar-based phantom (6% w/v), and (b) Timeseries temperature increase during sonications, as calculated using the default proton resonance frequency coefficient

temperature of 37°C, derived with MR thermometry using either the corresponding calibrated or default PRF coefficients, resulting the different ultrasonic protocols performed on the three agar-based phantoms developed with varied agar concentrations and the four agar-based phantoms (6% w/v) having varied concentrations of silicon dioxide, respectively. Generally, for the seven phantoms, irrespective of varied agar or silicon dioxide concentrations or the varied applied acoustical power, thermometry-based temperature change estimations based on the corresponding calibrated PRF coefficients were higher compared to equivalent temperature changes estimated utilizing the default PRF coefficient.

Discussion

In this study, the PRF temperature coefficient of several agar-based phantoms was calibrated following a series of HIFU sonications executed within a laboratory setting and inside a clinical 3 T MRI environment. Particularly, the HIFU exposures were controlled with an in-house software that also provides PRF MR thermometry monitoring[56] and were executed with an MRgFUS robotic system[49] integrated with a single-element concave transducer operating at 2.75 MHz that was chosen from a range of previously developed devices dedicated to preclinical MRgFUS studies.[49-55] Agar was preferred as a gelling agent for the development of phantoms employed herein, following its popularity in the fabrication process of phantoms dedicated to HIFU feasibility studies attributed to its ability to withstand the high temperatures induced by exposures[4] and accurately mimicking specific human tissues upon the employment of additional inclusions.[18,19] In this regard, seven phantoms were fabricated in the present study with varied agar (2, 4, and 6% w/v) and silicon dioxide (2, 4, 6, and 8% w/v) concentrations following previous studies that revealed that appropriate concentrations of these materials result in phantoms that accurately mimic the acoustic, thermal,[6,19,22,23] and magnetic[20] properties of certain biological tissues. While previous studies have primarily focused on the independent effect of the varied agar and silicon dioxide concentrations on the acoustic[6,19] and magnetic[20] properties of the developed phantoms, the current study investigated the effect of the varied concentrations of the phantom inclusions on the PRF temperature coefficient, and thus the temperature dependence of the phase shifts of the MR signal.

In this regard, the PRF coefficient of each phantom fabricated with varied agar or silicon dioxide concentrations was calibrated utilizing a method that has repeatedly been reported in the literature, wherein the parameter is calculated based on the PRF technique,[26,27] from linear relations between the phase and temperature changes induced resulting thermal exposure of the investigated tissue within an MRI environment.[28-38]

Table 4: Temperature changes resulting sonications executed with a 2.75 MHz transducer on agar-based phantoms having varied agar concentrations using varied acoustical power for a sonication time of 30 s at 25 mm focal depth as calculated with proton resonance frequency magnetic resonance thermometry by utilising calibrated or default proton resonance frequency coefficients of each phantom

Phantom (% w/v agar)	Acoustic power (W)	Maximum ΔT with calibrated PRF coefficient (°C)	Maximum ΔT with default PRF coefficient (°C)	Difference (ΔT with calibrated PRF/ΔT with default PRF)
2	18	13.1	6.4	2.05
	24	20.8	10.1	2.06
	30	30.5	16.7	1.83
	36	41.1	21.6	1.90
	42	48.8	26.1	1.87
4	18	26.6	9.5	2.8
	24	36.9	13.2	
	30	47.8	17.1	
	36	60.9	20.2	3.01
	42	68.3	24.4	2.8
6	18	18.9	13.1	1.44
	24	21.6	14.9	1.45
	30	26	18	1.44
	36	32.3	22.3	1.45
	42	37.1	25.6	

PRF: Proton resonance frequency

Table 5: Temperature changes resulting sonications executed with a 2.75 MHz transducer on agar-based phantoms doped with varied concentrations of silicon dioxide using varied acoustical power for a sonication time of 30 s at 25 mm focal depth as calculated with proton resonance frequency magnetic resonance thermometry by utilizing calibrated or default proton resonance frequency coefficients of each phantom

Agar=6% w/v, silica content (% w/v)	Acoustic power (W)	Maximum ΔT with calibrated PRF coefficient (°C)	Maximum ΔT with default PRF coefficient (°C)	Difference (ΔT with calibrated PRF/ΔT with default PRF)
2	18	24.5	21.1	1.16
	24	28.9	24.9	
	30	32.6	28	
	36	35.6	30.7	
	42	34.1	29.3	
4	18	23.9	20.7	1.15
	24	28.8	24.8	1.16
	30	32.5	28	
	36	34.6	29.9	
	42	37.6	32.4	
6	18	18.7	18.6	1.01
	24	25.1	25	
	30	28.8	28.6	
	36	31.2	31	
	42	32.5	32.3	
8	18	22.3	20.6	1.08
	24	30.1	27.8	
	30	34.2	31.6	
	36	37	34.2	
	42	37.6	34.7	

PRF: Proton resonance frequency

Specifically, a series of sonications executed at varied acoustic power (18–42 W) was comparably performed on each of the fabricated phantoms within the 3T MRI, while concurrently being scanned with a FLASH sequence. Phase shifts resulting each varied ultrasonic protocol executed on each of the different phantoms were derived in a plane perpendicular to the ultrasonic beam propagation (coronal plane) after careful postprocessing of the acquired MRI scans. Contrary to most literature studies[28-31,41-47] that interstitially insert temperature sensors in the investigated material during MRI-based thermal

heating of the targeted subject for simultaneous acquisition of temperatures and phase shifts, in the current study, thermocouple-based temperature change measurements were acquired in a plane perpendicular to the propagation of the beam from identical benchtop ultrasonic sonications that were executed on each of the various phantoms inside the laboratory setting. This approach was followed to prevent artifacts inadvertently arising on the MR images due to thermocouple presence within the phantom that could potentially impact phase shift measurements. Nevertheless, providing that the developed agar-based phantoms exhibit excellent thermal repeatability[6] and that special structures were employed allowing ablation of each phantom at corresponding locations during benchtop and MRI-based sonications, temperature changes derived in the laboratory setting were comparable to phase shifts arising from the MR images for each sonication and phantom.

As expected, sonications at increased acoustic power induced increased temperatures within either of the developed agar-based phantoms, that in turn resulted in higher phase shifts, thus being in accordance with previous studies performed in different magnetic field strength scanners where a proportional dependency of phase shift with temperature change was observed.[30,39,40,42] Consequently, for either the agar-based (2, 4, or 6% w/v agar) or agar-based (6% w/v) doped with silicon dioxide (2, 4, 6, or 8% w/v silicon dioxide) phantoms, least-squares linear regression confirmed this proportional dependency of the phase shift with the temperature change induced resulting the varied ultrasonic protocols comparably executed on each of the phantoms. Notably, induced phase shifts over the temperature changes indicatively presented for a purely agar-based phantom (6% w/v) and the corresponding agar-based phantom doped with silicon dioxide (6% w/v agar and 6% w/v silicon dioxide), approximated the range of phase shift measurements reported over equivalent temperature changes for other agar-based phantoms in different magnetic field strength scanners,[30,39,42] thus indicating the accuracy of the experimental procedure employed in the present study.

Upon validating a very strong linear phase and temperature change dependency (R^2 = 0.9707–0.9991) for each of the phantoms employed herein, being in agreement with similar trends reported in the literature,[39-48] the PRF coefficient was individually calibrated for each phantom. Particularly, for the phantoms fabricated with varied agar concentrations (2, 4, or 6% w/v), PRF coefficients in the range of −0.00336 ± 0.00029 to −0.00649 ± 0.0001 ppm/°C were reported, increasing for agar concentrations up to 4% w/v and decreasing for subsequently higher concentrations of agar. Accordingly, PRF coefficients between −0.00809 ± 0.00069 and −0.00934 ± 0.00050 ppm/°C were calibrated for the agar-based phantoms (6% w/v) developed with varied concentrations of silicon dioxide (2, 4, 6, or 8% w/v), generally decreasing with an increased silicon dioxide concentration, with this effect sustained for silicon dioxide concentrations up to 6% w/v. In this regard, by following linear regression analysis, a relatively weak (R^2 = 0.3741) inverse linear dependency of the PRF coefficient was observed with an increased concentration of agar, decreasing by −0.0005 ppm/°C for a unit increase in the % w/v agar concentration. Nevertheless, the effect on the PRF coefficient for agar concentrations above 6% w/v was not investigated since these would result in extremely stiff phantoms that would not mechanically resemble human tissue.[19] In this regard, the 6% w/v agar concentration was chosen for the development of phantoms doped with varied concentrations of silicon dioxide (2, 4, 6, or 8% w/v) where contrary, a strong (R^2 = 0.7159) negative linear effect on the PRF coefficient was observed with an increased concentration of silicon dioxide. Approximately a 25% decrease in the PRF coefficient was observed for the addition of 2% w/v silicon dioxide in the phantom (−0.00809 ± 0.00069 ppm/°C) compared to the corresponding value of the PRF coefficient (−0.00649 ± 0.0001 ppm/°C) of the purely agar-based phantom (6% w/v agar), with further decreases observed for increased silicon dioxide concentrations thereafter. Specifically, it was perceived that a unit increase in the % w/v concentration of silicon dioxide induced a −0.0003 ppm/°C decrease in the PRF coefficient.

Upon calibrating the PRF coefficient of each of the seven phantoms, the in-house control software was employed for offline PRF-based MR thermometry[26,27] of the varied ultrasonic exposures. Particularly, for each varied ultrasonic protocol executed on each phantom, color-coded thermal maps and timeseries temperature plots were successfully generated showing the extent of thermal heating throughout the phantom (through overlay of the thermal map on the corresponding magnitude scans) and the temperature increase at the focal spot (specific ROI within the phantom), respectively. Notably, MR thermometry data for the individual sonications executed on each phantom were effectively generated by employing the corresponding calibrated PRF coefficient of the phantom as well as a default PRF coefficient value (−0.0094 ppm/°C) that is typically used by the in-house software for MR thermometry calculations, to assess the effect of the PRF coefficient on the MR thermometry-based temperature measurements. Inherently, for either phantoms developed with varied agar (2, 4, or 6% w/v) or silicon dioxide (2, 4, 6, or 8% w/v) concentrations, higher temperature changes were produced by employing the corresponding calibrated PRF coefficients compared to data derived with the default PRF coefficient value. Specifically, for the three phantoms having varied agar concentrations (2, 4, or 6% w/v), temperature changes in the range of 13.1°C–68.3°C were derived using the calibrated PRF coefficients, indicating a 1.44-fold to 3.01-fold increase relative to temperature elevations (6.4°C–25.6°C) arising with the default PRF coefficient. Interestingly, for the four agar-based phantoms developed with varied concentrations of silicon dioxide (2, 4, 6, or 8% w/v), smaller differences between temperature changes derived utilizing either the default or corresponding calibrated PRF coefficients were observed. Particularly, a 1.01-fold to

1.16-fold decrease in the temperature changes (18.6°C–34.7°C) was observed using the default PRF coefficient, compared to corresponding MR thermometry-based temperature changes (18.7°C–37.6°C) derived utilizing the calibrated PRF coefficients, with temperature changes generated with either PRF coefficient (default or calibrated) for identical applied acoustical power being approximately similar at higher concentrations of silicon dioxide.

Generally, the PRF coefficients as calculated in the present study for the three agar-based phantoms developed with varied agar concentrations (−0.00336 ± 0.00029– −0.00649 ± 0.0001 ppm/°C) were slightly higher than calibrated PRF coefficients reported in the literature for other phantoms developed with an agar base[28,29,39-42] or using alternative gelling agents.[43-47] When considering the corresponding uncertainties for each PRF coefficient calculated herein, the confidence interval for the PRF coefficients of the three phantoms fabricated with varied agar concentrations (lower value of −0.00307 ppm/°C for the phantom having 4% w/v agar concentration, and maximum value of −0.00659 ppm/°C for the phantom developed with 6% w/v concentration of agar) was still higher than PRF coefficients reported in literature studies for various types of phantoms.[28,29,39-47] Nevertheless, PRF coefficient calibrations have shown to be dependent on the parameters of the employed MR pulse sequence,[28,41] while inclusion of other dopants has frequently been utilized in an agar-base,[29,39,41] thus potentially explaining any deviations observed in the calibrated coefficients of the pure agar-based phantoms of the present study from similar studies found in the literature.[28,29,39-42]

Interestingly, the PRF coefficient of the phantom developed with a 6% w/v concentration of agar (−0.00649 ± 0.0001 ppm/°C) well agrees with the PRF coefficient of *in vivo* rabbit muscle tissue (−0.007 ± 0.001 ppm/°C) when accounting for experimental uncertainties reported in the study by Mulkern *et al*.[31] Moreover, if uncertainties (0.0001 ppm/°C) for the PRF coefficient of the 6% w/v agar phantom are considered, then the maximum value for the PRF coefficient (−0.00659 ppm/°C) of the corresponding phantom is marginally lower (2%–5%) than PRF coefficients reported for *in vivo* canine brain and muscle tissues,[34] and approximates the lower range of PRF coefficients reported for *ex vivo* porcine liver.[39] Notably, addition of varied concentrations of silicon dioxide (2, 4, 6, or 8% w/v) in the corresponding agar-base (6% w/v) resulted in calibrated PRF coefficients for the four phantoms (−0.00809 ± 0.00069– −0.00934 ± 0.00050 ppm/°C) that well approximated the range of PRF coefficients of various *in vivo* [29-33,36-38] as well as *ex vivo*[28,39] animal tissues. It is worth stating that this comparison considers the complete range of calibrated PRF coefficients for the four phantoms (−0.0074 to −0.00984 ppm/°C) contemplating for corresponding errors in PRF coefficient measurements, and accounting for uncertainties reported in the PRF coefficients of animal tissues in literature studies.[28-33,36-39]

Nevertheless, PRF coefficient calibrations as executed for the seven agar-based phantoms in this study are still characterized by some limitations. Primarily, possible magnetic field drifts occurring due to temporal instability of the MRI scanner that result in nontemperature induced phase shifts,[27] which could had potentially hampered presented phase shift measurements were not considered. Generally, such phase shifts are compensated for in PRF coefficient calibrations by including reference phantoms and subtracting from the phase changes induced in the thermally exposed investigated tissue the nontemperature induced phase shifts arising in the reference phantoms over the course of the experiments within the MRI environment.[28,30,34,37,39,40,48] However, considering that clinical MRI scanners nowadays are stable[27] with previous studies reporting a relative stability in phase drift for several hours,[34,36,37] we would expect only minimal phase shifts arising due to MRI instability during the 60 s time required for imaging each phantom in this study. Moreover, noise in phase images is dependent on the SI of corresponding magnitude images, with optimal signal-to-noise-ratio achieved when the TE employed for imaging is identical to the T2* relaxation time of the imaged tissue.[27,28,34,36] A previous study at 3T[59] reports a T2* relaxation time of 21.7 ms for a purely agar-based phantom having a 6% w/v agar concentration that decreases to 18.5 ms for the addition of 4% w/v silicon dioxide in the corresponding agar base (6% w/v). Although the range of T2* relaxation times for all phantom recipes investigated in this study remains to be investigated, this suggests that the TE of 10 ms that was employed for the FLASH sequence in the current study could possibly be slightly short for imaging the seven agar-based phantoms. Consequently, increased sensitivity in phase shift measurements and ultimately in the calibrated PRF coefficients could be achieved in future by using a longer TE.

Given the increased employment of agar-based phantoms doped with silicon dioxide in HIFU validation studies[18-20,22,23] and based on the present results, phantoms developed with a 6% w/v concentration of agar and doped with 0%–8% w/v concentration of silicon dioxide best approximate the PRF coefficient of several animal tissues[29-34,36-39] and should therefore be considered in future MRgFUS validation studies as tissue mimicking materials since other concentrations of gel inclusions than the abovementioned, result in phantoms with a PRF coefficient that extremely deviates from corresponding tissue coefficients.[29-34,36-39] Furthermore, PRF coefficients as calibrated for each of the seven phantoms in the present study could be utilized in PRF-based MR thermometry calculations during evaluation studies of future MRgFUS systems, resulting in a more accurate MR thermometry monitoring of the temperature increase, therefore providing enhanced insights on the actual efficacy of the developed system.

Financial support and sponsorship

The study has been co-funded by the European Structural and Investment Funds (ESIF) and the Republic of Cyprus through the Research and Innovation Foundation (RIF) under the projects SOUNDPET (INTEGRATED/0918/0008),

FUSROBOT (ENTERPRISES/0618/0016), and FUSVET (SEED/1221/0080).

Conflicts of interest

There are no conflicts of interest.

References

1. Mobashsher AT, Abbosh AM. Artificial human phantoms: Human proxy in testing microwave apparatuses that have electromagnetic interaction with the human body. IEEE Microw Mag 2015;16:42-62.
2. McGarry CK, Grattan LJ, Ivory AM, Leek F, Liney GP, Liu Y, *et al.* Tissue mimicking materials for imaging and therapy phantoms: A review. Phys Med Biol 2020;65:23TR01. [doi: 10.1088/1361-6560/abbd17.4].
3. Culjat MO, Goldenberg D, Tewari P, Singh RS. A review of tissue substitutes for ultrasound imaging. Ultrasound Med Biol 2010;36:861-73.
4. Dabbagh A, Abdullah BJ, Ramasindarum C, Abu Kasim NH. Tissue-mimicking gel phantoms for thermal therapy studies. Ultrason Imaging 2014;36:291-316.
5. Siedek F, Yeo SY, Heijman E, Grinstein O, Bratke G, Heneweer C, *et al.* Magnetic resonance-guided high-intensity focused ultrasound (MR-HIFU): Technical background and overview of current clinical applications (Part 1). Rofo 2019;191:522-30.
6. Menikou G, Damianou C. Acoustic and thermal characterization of agar based phantoms used for evaluating focused ultrasound exposures. J Ther Ultrasound 2017;5:14.
7. Antoniou A, Damianou C. MR relaxation properties of tissue-mimicking phantoms. Ultrasonics 2022;119:106600.
8. Lafon C, Zderic V, Noble ML, Yuen JC, Kaczkowski PJ, Sapozhnikov OA, *et al.* Gel phantom for use in high-intensity focused ultrasound dosimetry. Ultrasound Med Biol 2005;31:1383-9.
9. Eranki A, Mikhail AS, Negussie AH, Katti PS, Wood BJ, Partanen A. Tissue-mimicking thermochromic phantom for characterization of HIFU devices and applications. Int J Hyperthermia 2019;36:518-29.
10. McDonald M, Lochhead S, Chopra R, Bronskill MJ. Multi-modality tissue-mimicking phantom for thermal therapy. Phys Med Biol 2004;49:2767-78.
11. Iizuka MN, Sherar MD, Vitkin IA. Optical phantom materials for near infrared laser photocoagulation studies. Lasers Surg Med 1999;25:159-69.
12. Takegami K, Kaneko Y, Watanabe T, Maruyama T, Matsumoto Y, Nagawa H. Polyacrylamide gel containing egg white as new model for irradiation experiments using focused ultrasound. Ultrasound Med Biol 2004;30:1419-22.
13. Choi MJ, Guntur SR, Lee KI, Paeng DG, Coleman A. A tissue mimicking polyacrylamide hydrogel phantom for visualizing thermal lesions generated by high intensity focused ultrasound. Ultrasound Med Biol 2013;39:439-48.
14. Bini MG, Ignesti A, Millanta L, Olmi R, Rubino N, Vanni R. The polyacrylamide as a phantom material for electromagnetic hyperthermia studies. IEEE Trans Biomed Eng 1984;31:317-22.
15. Madsen EL, Frank GR, Krouskop TA, Varghese T, Kallel F, Ophir J. Tissue-mimicking oil-in-gelatin dispersions for use in heterogeneous elastography phantoms. Ultrason Imaging 2003;25:17-38.
16. Farrer AI, Odéen H, de Bever J, Coats B, Parker DL, Payne A, *et al.* Characterization and evaluation of tissue-mimicking gelatin phantoms for use with MRgFUS. J Ther Ultrasound 2015;3:9.
17. Hofstetter LW, Fausett L, Mueller A, Odéen H, Payne A, Christensen DA, *et al.* Development and characterization of a tissue mimicking psyllium husk gelatin phantom for ultrasound and magnetic resonance imaging. Int J Hyperthermia 2020;37:283-90.
18. Partanen A, Mougenot C, Vaara T. Feasibility of agar-silica phantoms in quality assurance of MRgHIFU. AIP Conf Proc 2009;1113:296-300.
19. Drakos T, Antoniou A, Evripidou N, Alecou T, Giannakou M, Menikou G, *et al.* Ultrasonic attenuation of an Agar, Silicon Dioxide, and evaporated milk gel phantom. J Med Ultrasound 2021;29:239-49.
20. Antoniou A, Georgiou L, Christodoulou T, Panayiotou N, Ioannides C, Zamboglou N, *et al.* MR relaxation times of agar-based tissue-mimicking phantoms. J Appl Clin Med Phys 2022;23:e13533.
21. Filippou A, Louca I, Damianou C. Characterization of a fat tissue mimicking material for high intensity focused ultrasound applications. J Ultrasound 2023;26:505-15.
22. Menikou G, Dadakova T, Pavlina M, Bock M, Damianou C. MRI compatible head phantom for ultrasound surgery. Ultrasonics 2015;57:144-52.
23. Menikou G, Yiannakou M, Yiallouras C, Ioannides C, Damianou C. MRI-compatible breast/rib phantom for evaluating ultrasonic thermal exposures. Int J Med Robot Comput Assist Surg 2018;14:1-12.
24. Drakos T, Giannakou M, Menikou G, Constantinides G, Damianou C. Characterization of a soft tissue-mimicking agar/wood powder material for MRgFUS applications. Ultrasonics 2021;113:106357.
25. González Hernando C, Esteban L, Cañas T, Van den Brule E, Pastrana M. The role of magnetic resonance imaging in oncology. Clin Transl Oncol 2010;12:606-13.
26. Rieke V, Butts Pauly K. MR thermometry. J Magn Reson Imaging 2008;27:376-90.
27. Odéen H, Parker DL. Magnetic resonance thermometry and its biological applications – Physical principles and practical considerations. Prog Nucl Magn Reson Spectrosc 2019;110:34-61.
28. Peters RD, Hinks RS, Henkelman RM. *Ex vivo* tissue-type independence in proton-resonance frequency shift MR thermometry. Magn Reson Med 1998;40:454-9.
29. Demura K, Morikawa S, Murakami K, Sato K, Shiomi H, Naka S, *et al.* An easy-to-use microwave hyperthermia system combined with spatially resolved MR temperature maps: Phantom and animal studies. J Surg Res 2006;135:179-86.
30. Botnar RM, Steiner P, Dubno B, Erhart P, von Schulthess GK, Debatin JF. Temperature quantification using the proton frequency shift technique: *In vitro* and *in vivo* validation in an open 0.5 tesla interventional MR scanner during RF ablation. J Magn Reson Imaging 2001;13:437-44.
31. Mulkern RV, Chung AH, Jolesz FA, Hynynen K. Temperature monitoring of ultrasonically heated muscle with RARE chemical shift imaging. Med Phys 1997;24:1899-906.
32. Sherar MD, Moriarty JA, Kolios MC, Chen JC, Peters RD, Ang LC, *et al.* Comparison of thermal damage calculated using magnetic resonance thermometry, with magnetic resonance imaging post-treatment and histology, after interstitial microwave thermal therapy of rabbit brain. Phys Med Biol 2000;45:3563-76.
33. Moriarty JA, Chen JC, Purcell CM, Ang LC, Hinks RS, Peters RD, *et al.* MRI monitoring of interstitial microwave-induced heating and thermal lesions in rabbit brain *in vivo*. J Magn Reson Imaging 1998;8:128-35.
34. MacFall JR, Prescott DM, Charles HC, Samulski TV. 1H MRI phase thermometry *in vivo* in canine brain, muscle, and tumor tissue. Med Phys 1996;23:1775-82.
35. Muacevic A, Peller M, Ruprecht L, Berg D, Fend L, Sroka R, *et al.* Image guided interstitial laser thermotherapy: A canine model evaluated by magnetic resonance imaging and quantitative autoradiography. Acta Neurochir (Wien) 2005;147:175-85.
36. Chung AH, Jolesz FA, Hynynen K. Thermal dosimetry of a focused ultrasound beam *in vivo* by magnetic resonance imaging. Med Phys 1999;26:2017-26.
37. Chen L, Wansapura JP, Heit G, Butts K. Study of laser ablation in the *in vivo* rabbit brain with MR thermometry. J Magn Reson Imaging 2002;16:147-52.
38. Vykhodtseva N, Sorrentino V, Jolesz FA, Bronson RT, Hynynen K. MRI detection of the thermal effects of focused ultrasound on the brain. Ultrasound Med Biol 2000;26:871-80.
39. Olsrud J, Wirestam R, Brockstedt S, Nilsson AM, Tranberg KG, Ståhlberg F, *et al.* MRI thermometry in phantoms by use of the proton resonance frequency shift method: Application to interstitial laser thermotherapy. Phys Med Biol 1998;43:2597-613.
40. Peters RD, Hinks RS, Henkelman RM. Heat-source orientation and geometry dependence in proton-resonance frequency shift magnetic resonance thermometry. Magn Reson Med 1999;41:909-18.
41. Peters RD, Chan E, Trachtenberg J, Jothy S, Kapusta L, Kucharczyk W, *et al.* Magnetic resonance thermometry for predicting thermal damage:

An application of interstitial laser coagulation in an *in vivo* canine prostate model. Magn Reson Med 2000;44:873-83.
42. Wang P. Evaluation of MR thermometry with proton resonance frequency method at 7T. Quant Imaging Med Surg 2017;7:259-66.
43. Vitkin IA, Moriarty JA, Peters RD, Kolios MC, Gladman AS, Chen JC, *et al.* Magnetic resonance imaging of temperature changes during interstitial microwave heating: A phantom study. Med Phys 1997;24:269-77.
44. Bazrafshan B, Hübner F, Farshid P, Hammerstingl R, Paul J, Vogel V, *et al.* Temperature imaging of laser-induced thermotherapy (LITT) by MRI: Evaluation of different sequences in phantom. Lasers Med Sci 2014;29:173-83.
45. Lochhead S, Bradwell D, Chopra R, Bronskill MJ. A gel phantom for the calibration of MR-guided ultrasound thermal therapy. Proc IEEE Ultrason Symp 2004;2:1481-3.
46. Yuan Y, Wyatt C, Maccarini P, Stauffer P, Craciunescu O, Macfall J, *et al*. A heterogeneous human tissue mimicking phantom for RF heating and MRI thermal monitoring verification. Phys Med Biol 2012;57:2021-37.
47. Tarasek MR, Pellicer R, Hofstetter LW, Numan WC, Bakker JF, Kotek G, *et al.* Validation of MR thermometry: Method for temperature probe sensor registration accuracy in head and neck phantoms. Int J Hyperthermia 2014;30:142-9.
48. De Poorter J, De Wagter C, De Deene Y, Thomsen C, Ståhlberg F, Achten E. The proton-resonance-frequency-shift method compared with molecular diffusion for quantitative measurement of two-dimensional time-dependent temperature distribution in a phantom. J Magn Reson B 1994;103:234-41.
49. Giannakou M, Antoniou A, Damianou C. Preclinical robotic device for magnetic resonance imaging guided focussed ultrasound. Int J Med Robot Comput Assist Surg 2022;19:e2466.
50. Drakos T, Giannakou M, Menikou G, Filippou A, Evripidou N, Spanoudes K, *et al.* MRI-guided focused ultrasound robotic system for preclinical use. J Vet Med Anim Sci 2020;4:1049.
51. Drakos T, Giannakou M, Menikou G, Damianou C. Magnetic resonance imaging-guided focused ultrasound positioning system for preclinical studies in small animals. J Ultrasound Med 2021;40:1343-52.
52. Spanoudes K, Evripidou N, Giannakou M, Drakos T, Menikou G, Damianou C. A high intensity focused ultrasound system for veterinary oncology applications. J Med Ultrasound 2021;29:195-202.
53. Giannakou M, Drakos T, Menikou G, Evripidou N, Filippou A, Spanoudes K, *et al.* Magnetic resonance image-guided focused ultrasound robotic system for transrectal prostate cancer therapy. Int J Med Robot Comput Assist Surg 2021;17:e2237.
54. Antoniou A, Giannakou M, Evripidou N, Stratis S, Pichardo S, Damianou C. Robotic system for top to bottom MRgFUS therapy of multiple cancer types. Int J Med Robot Comput Assist Surg 2022;18:e2364.
55. Giannakou M, Menikou G, Ioannides K, Damianou C. Magnetic resonance-image-guided focused ultrasound robotic system with four computer-controlled axes with endorectal access designed for prostate cancer focal therapy. Digit Med 2020;6:32-43.
56. Filippou A, Georgiou A, Nikolaou A, Evripidou N, Damianou C. Advanced software for MRgFUS treatment planning. Comput Methods Programs Biomed 2023;240:107726.
57. de Zwart JA, Vimeux FC, Delalande C, Canioni P, Moonen CT. Fast lipid-suppressed MR temperature mapping with echo-shifted gradient-echo imaging and spectral-spatial excitation. Magn Reson Med 1999;42:53-9.
58. Bing C, Staruch RM, Tillander M, Köhler MO, Mougenot C, Ylihautala M, *et al.* Drift correction for accurate PRF-shift MR thermometry during mild hyperthermia treatments with MR-HIFU. Int J Hyperthermia 2016;32:673-87.
59. Antoniou A, Evripidou N, Georgiou L, Chrysanthou A, Ioannides C, Damianou C. Tumor phantom model for MRI-guided focused ultrasound ablation studies. Med Phys 2023;50:5956-68.